5-2021

Experimental Investigation of Spray Cooling/Heating of a Near-Isothermal Hydro-Pneumatic Energy Storage System

Saiid Kassaee
University of Tennessee, Knoxville, skassaee@vols.utk.edu

Recommended Citation

To the Graduate Council:

I am submitting herewith a thesis written by Saiid Kassaee entitled "Experimental Investigation of Spray Cooling/Heating of a Near-Isothermal Hydro-Pneumatic Energy Storage System." I have examined the final electronic copy of this thesis for form and content and recommend that it be accepted in partial fulfillment of the requirements for the degree of Master of Science, with a major in Mechanical Engineering.

Matthew M. Mench, Major Professor

We have read this thesis and recommend its acceptance:

Matthew M. Mench, Kenneth D. Kihm, Doug Aaron

Accepted for the Council:
Dixie L. Thompson

Vice Provost and Dean of the Graduate School

(Original signatures are on file with official student records.)

Experimental Investigation of Spray Cooling/Heating of a Near-Isothermal Hydro-Pneumatic
Energy Storage System

A Thesis Presented for the

Master of Science

Degree

The University of Tennessee, Knoxville

Saiid Kassaee

May 2021

It is always sunny above the dark clouds, if you fly high enough.

Abstract

Proposing experimental investigation of spray cooling/heating of a near-isothermal, scalable, efficient, high density, hydro-pneumatic integrated energy storage system; capable of spray cooling/heating during gas compression/expansion and capable of excess heat integration. The invented Ground-Level Integrated Diverse Energy Storage (GLIDES) is an energy storage technology capable of storing energy in high-pressure vessel using hydro-pneumatic concept. Indicated roundtrip efficiencies of 98% can be reached using the proposed technology marking an isothermal compression/expansion energy storage.

Table of Contents

List of Tables

List of Figures

Nomenclature

Abbreviations

Bcf	Billion cubic feet
CAES	Compressed air energy storage
CF	Carbon fiber
DOE	Department of energy
ED	Energy density [kWh/m^3]
FBES	Flow battery energy storage
FES	Flywheel energy storage
GLIDES	Ground-level integrated diverse energy storage
LIB	Lithium-ion battery
ORNL	Oak Ridge national laboratory
PD	Positive displacement
PSH	Pumped storage hydroelectricity
RTE	Roundtrip efficiency

Subscripts

amb	of ambient air
avg	average
g	of gas
i	inner
l	of liquid
max	maximum
min	minimum
o	outer
t	of tank walls
v	at constant volume

Symbols

A	Heat transfer area [m^2]
c	Specific heat capacity [$J/kg.K$]
E	Energy [kWh/m^3]
G	Generator
h	Heat transfer coefficient [W/m^2K]
m	Mass [kg]
M	Motor
$\dot{m}$	Mass flow rate [kg/s]
n	Polytropic constant
p	Pressure [bar]
t	Time [s]
T	Temperature [K]
V	Volume m^3
ρ	Density [kg/m^3]
η	Efficiency

Chapter 1: Introduction/Problem Statement

Grid modernization is vital to the nation's safety, economy, and modern way of life. Grid modernization can reduce the societal cost of power outage by more than 10%, decrease the cost of reserve margins by 33%, and reduce the cost of wind and solar integration by 50%, providing more than $7 billion in annual benefits for the US economy [1]. On the other hand, with the increase in the release of greenhouse gases into the atmosphere and their effect on the environment, the shift from fossil fuels to renewable energies is more critical now than ever before. In 2017, around 63% of the world's total electricity production was from fossil fuels, 20% from nuclear energy and around 17% from renewable energy sources [2].

Based on the Renewables 2018 Global Status Report by the Renewable Energy Policy Network for the 21st Century (REN21), with the commitment to phase out coal power by 2030, more than 20 countries including Italy, Mexico, and the United Kingdom launched the Powering Coal Alliance in 2017. Along with these countries in 2017, China, the United States, and Europe provided nearly 75% of the total global investment in renewable power and fuels [3]. The challenge with renewable energies is the variability in their output, which is due to their availability (e.g., lack of sunlight at night or lack of wind). Given the unpredictability of electricity demand, the output variability of the renewable energies, and the need for a power supply to meet the demand, the concept of energy storage is introduced.

Given the limitations associated with intermittent renewable energies and to avoid grid instability, developing low-cost, efficient energy storage systems is critical and can provide many benefits. For example, energy from renewable sources, such as wind and solar, can be stored when available and used when those sources are unavailable or the price of electricity is high (peak shaving); stored when the demand is lower than the supply, such as nights when low-cost power plants

continue to operate. Peak shaving is a technique used to reduce power consumption during high-demand periods and has the potential to lower the consumer's electric bill. Energy storage technologies can both discharge power quickly and slowly depending on the technology. Energy storage is valuable in grid stabilization, beneficial in electric vehicles, during power outages, in natural disasters, and in areas located away from the grid (e.g., islands and microgrids). To date, there are 1,267 energy storage projects worldwide with a total of around 171 *GW* of energy storage, with electrochemical technology (batteries) as the leading technology with the highest number of projects [4].

1.1 State-of-the-art Energy Storage Systems

To promote the integration of the expected growth in renewables into the electricity generation mix and grid modernization, various energy storage technologies have been developed. These technologies can be classified into four major categories: mechanical, electrical, chemical, and electrochemical [5]. The main characteristics used to compare energy storage technologies are rated power, energy capacity, energy density (ED), round-trip efficiency (RTE), and energy cost in *$/kWh*. Rated power is the maximum instantaneous power the system can output (*kW, MW, GW, etc.*); however, since the energy stored in the system is finite, the time in which the system can output the maximum instantaneous power until all energy is discharged plays an important role. Energy capacity is the numerical integration of the instantaneous power over the time it takes to completely discharge the energy stored in the system. Energy density (ED) is the amount of energy stored per unit of volume of the storage system. Roundtrip efficiency (RTE) is the ratio of the total energy that can be extracted from the system through discharging, to the energy needed to charge the system to its full energy capacity. Many energy storage technologies have been deployed to

date. Some of the existing technologies include but are not limited to those discussed below. The technical and economical characteristics of these energy storage technologies are included in Table 1.

1.1.1 Mechanical Energy Storage

Some of the mechanical energy storage technologies include Pumped Hydroelectric Storage (PHS), Compressed Air Energy Storage (CAES), and Flywheel Energy Storage (FES).

1.1.1.1 Pumped Hydroelectric Storage (PHS)

Pumped hydroelectric storage is the most widely used large-scale electrical energy storage. PHS technology accounts for around 97% of the world's electricity storage [6]. This technology converts electrical energy to potential energy using two water reservoirs at different elevations, a unit to pump water to the higher elevation, and a turbine to generate electricity.

During charging, a hydraulic pump is used to pump water from a lower reservoir (e.g., a lake or river) to a higher water reservoir (e.g., pond). During discharge, the elevated water can be released back into the lower reservoir. The water spins a hydraulic turbine that drives an electric generator to generate electricity [7,8].

Pumped hydroelectric storage has a relatively low capital cost, high roundtrip efficiency, and more than 40 years lifetime. The capacity of this system solely depends on the difference in elevation between the two reservoirs and the size of the reservoirs. The main disadvantage of this technology is its limited expansion prospect in the United States because most of the favorable sites have already been developed. Pumped hydroelectric storage suffers from scalability, geographical limitations and lack of ability to use energy other than electricity for charging [7,8].

1.1.1.2 Compressed Air Energy Storage (CAES)

Compressed Air Energy Storage (CAES) stores electrical energy in the form of high-pressure air using gas compressors. The compressed air is stored in a container (i.e., underground caverns or aboveground tanks), and a multi-stage turbine is employed to dispatch the stored energy.

During charging, CAES use gas compressors to compress air into an underground cavern or aboveground pressure reservoir. During discharging, the compressed air is heated and expanded through a high-pressure gas turbine. The air is then mixed with fuel, and the mixture is combusted and expands through a low-pressure gas turbine. The low- and high- pressure turbines are connected through a common shaft to a generator to generate electricity. This technology is capable of using excess heat to boost the efficiency.

There are only two operating CAES systems in the world. Both systems are cavern based. The first ever CAES plant built is in Huntorf, Germany. It uses two salt dome-based caverns as the storage reservoirs. The other operating CAES is in the United States, in McIntosh, Alabama. It uses one salt dome–based cavern. CAES technology provides good part-load performance and a reasonable response speed. However, it suffers from low roundtrip efficiency due to the usage of gas compressors and geographical limitations. High construction cost is the major barrier to employing large-scale CAES plants [7,8].

1.1.1.3 Flywheel Energy Storage (FES)

Flywheels have been used for centuries to store energy in the form of kinetic energy. A flywheel energy storage system consists mainly of a flywheel, a reversible motor/generator, and an evacuated chamber. These systems can be classified as low and high speed. The flywheels themselves are usually made of steel and an advanced composite material such as carbon fiber.

During charging, the flywheel is spun by an electric motor. During discharging, the rotational energy of the flywheel is then used to spin the same motor, which now acts as a generator, to generate electricity.

The advantages of FES include long lifetime, high roundtrip efficiency, and relatively quick charging. Normally, FES systems can supply power for a short period of time. Therefore, they are not used as standalone backup power unless they are used with other energy storage technologies. Other disadvantages of this technology include idling losses during standby time and the need for a vacuum chamber. Flywheel malfunction during rotation is common and is usually caused by the propagation of cracks through the rotors [7–9]. This technology is also uncapable of using excess heat.

1.1.2   Electrochemical Energy Storage (Batteries)

Electrochemical energy storage technologies (batteries) have different chemistries and include lead acid, lithium ion, sodium-based, nickel-based, and flow batteries. The first large-scale battery storage installation in the United States entered service in 2003 using nickel-based and sodium-based batteries. By the end of 2017, 708 MW of large-scale battery storage was in operation in the United States [10]. Some of the Electrochemical Energy Storage technologies include but are not limited to Lead Acid Batteries, Lithium-ion Batteries, Sodium-Sulfur Batteries, and Flow Battery Energy Storage. Batteries also do not have a way of using excess heat.

1.1.2.1   Lead Acid Batteries

Lead acid batteries use two electrodes—one is composed of highly porous lead dioxide (PbO_2) and the other of finely divided metallic lead (Pb). The lead-dioxide electrode is the positive electrode, and the metallic lead is the negative electrode. The two electrodes are submerged in an

electrolyte solution of dilute aqueous sulfuric acid. The negative electrode reacts with the hydrogen sulfate ion (HSO_4^-) of the electrolyte and produces lead sulfate ($PbSO_4$), hydronium ions (H_3O^+), and electrons (e^-). The positive electrode reacts with the hydrogen sulfate ion of the electrolyte, hydronium ions, and electrons to produce lead sulfate and water.

Lead acid batteries are the most popular low-cost batteries. Their RTE is around 70%. The disadvantages of these batteries, compared to other battery technologies, include relatively low cycle life (50–500 cycles), and the possibility of corrosion [9].

1.1.2.2 *Lithium-ion Batteries*

Lithium-ion battery (LIB) technology is based on the use of lithium-intercalation compounds. A cathode, the electrode where a reduction reaction takes place and electrons enter the cell, is a lithiated metal oxide (an oxide due to higher potential) that is often characterized by a layered structure. An anode, where an oxidation reaction takes place, is made of graphitic carbon which holds lithium in its layers. Both electrodes are capable of reversibly inserting and removing lithium ions from their structure.

Lithium-ion batteries outperform other electrochemical energy storage technologies by a factor of 2.5 in terms of energy capacity while providing high specific power. Over the last decade, the energy density of lithium-ion batteries has improved from 100 kWh/m^3 to around 730 kWh/m^3 [11]. The high energy density, around 97% roundtrip efficiency, long life, and rapid charging of lithium-ion batteries have made them the first choice for powering electric vehicles [5,7,8]. Lithium-ion batteries suffer from degradation of maximum charge storage at high temperatures, thermal runaway and capacity loss when overcharged, and chemical and fire hazards [9].

Table 1, Technical and economical characteristics of energy storage technologies.

Technology	ED (kWh/m^3)	Rated (MWh)	Lifetime (Years)	RTE %	Discharge Time $(hours)$	Energy cost $(\$/kWh)$
PHS [14]	0.5–2	500–800	40–60	70–85	1–24, 6–10	5–100
CAES [14]	2–6	$\sim < 1000$, 580 & 2860	20–40	42–54	1–24, 8–20	2–120
Flywheel [14]	20–80	1000–2000	~15+	90–95	8 s, 15 s–15 min	1,000–5,000
Lead-acid [8,15]	50–100	0.001–40	5–15	63–90	< 10	120–600
Li-ion [8,11]	240–730	0.004–10	5–15	90–99	~1–8	150–1300
Na-S [15]	150–300	0.4–245	10–15	75–90	~1	250–500

Chapter 2: The Invented GLIDES Technology

Ground-Level Integrated Diverse Energy Storage (GLIDES) is an energy storage system that was invented at the Oak Ridge National Laboratory (ORNL) [16]. GLIDES stores energy by compression and expansion of air using water as a liquid piston inside high-pressure reservoirs. This system is a combination of CAES and PHS systems but is more efficient and has higher energy density than either technologies. As shown in Figure 1, the GLIDES system consists of a hydraulic motor, a hydraulic pump, high-pressure reservoirs (i.e., pressure vessels), a hydraulic turbine, and an electrical generator. The high-pressure reservoirs in this system are sealed vessels. These high-pressure reservoirs are pre-pressurized with air to a certain pressure. During charging, an electric motor is run which drives a positive displacement (PD) hydraulic pump. The pump pushes water into the pressurized reservoirs. With the water volume increasing inside the high-pressure reservoirs, the air above the water is compressed, causing its pressure to increase. During discharging, water is discharged from the vessels, causing the air above the water column to expand. The water flows through a hydraulic turbine that drives an electric generator, and electricity is generated. Other systems have been studied using GLIDES concept, but no prototypes have been built for those projects. Many of those projects are using adiabatic processes and to the author's knowledge, no project has achieved isothermal compression/expansion.

2.1 Proof-of-Concept Prototypes / Studied Configurations

Multiple lab-scale proof-of-concept prototypes of GLIDES have been built at ORNL since 2015 [17]. The first prototype was built with a system nominal size of 3 *kWh*. This system consisted of an ambient pressure water storage, electric motor, electric generator, PD hydraulic pump, four steel high-pressure vessels, and a hydraulic Pelton turbine. Use of a hydraulic PD pump and Pelton
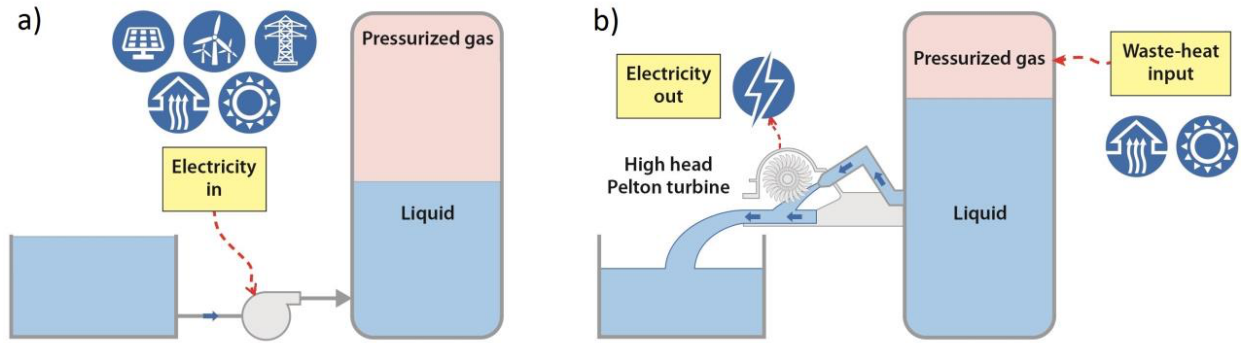
Figure 1, The invented GLIDES layout during (a) charging and (b) discharging [17].

turbine to charge/discharge the GLIDES system is one of the main advantages over CAES systems as no gas machinery used, resulting in much higher roundtrip efficiency. This system is only capable of charging from the bottom of the vessels. Some photos of the first prototype, a pressure-volume (P-V) diagram of a full cycle (charge, pause, discharge, pause), air temperature/pressure change vs time, and the losses associated with this prototype are shown in Figure 2-Figure 5.

As shown in Figure 2-Figure 5, based on the experimental data from the first-generation prototype, around 25% RTE is lost due to the turbomachinery used on the system and around 9% of the total efficiency losses is due to the losses during compression/expansion (area between the charging and discharging P-V diagram curve). The losses during the compression and expansion process are due to the increase and decrease in the air temperature respectively. If the process is assumed adiabatic (no heat transfer between the working air and the ambient), as the water volume increases (during charging), the air volume decreases causing the temperature and the pressure of the vessel to increase. The faster the air temperature increase (the lower the heat transfer to the ambient during charging), the faster the air pressure reaches the maximum operating pressure, therefore the lower volume of water pumped into the pressure vessel. This marks the worst-case scenario as the more water pumped into the vessel, the more water available to be used during the discharge process.

2.2 Thermodynamic Flexibility

Due to the large length scale (large-scale system) and long time scale (slow charging/discharging) seen in operation of the GLIDES system, it is possible to closely control the gas cycle and the associated heat transfer. As a result, the gas cycle can be controlled to mimic almost any major thermodynamic cycle found in the literature and also introduce opportunities for introducing even
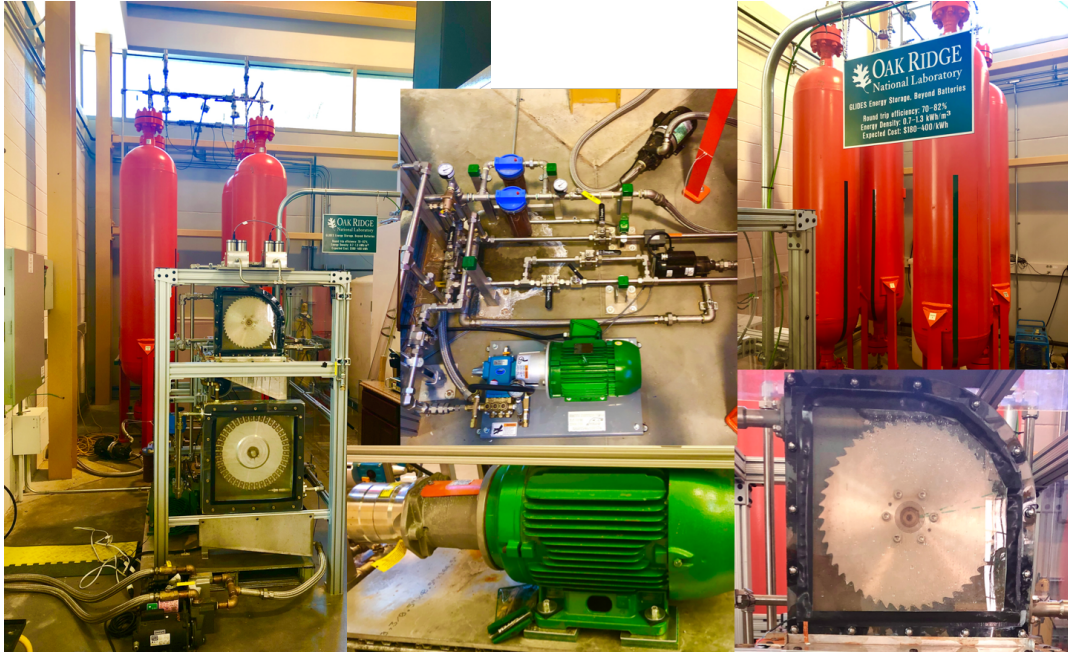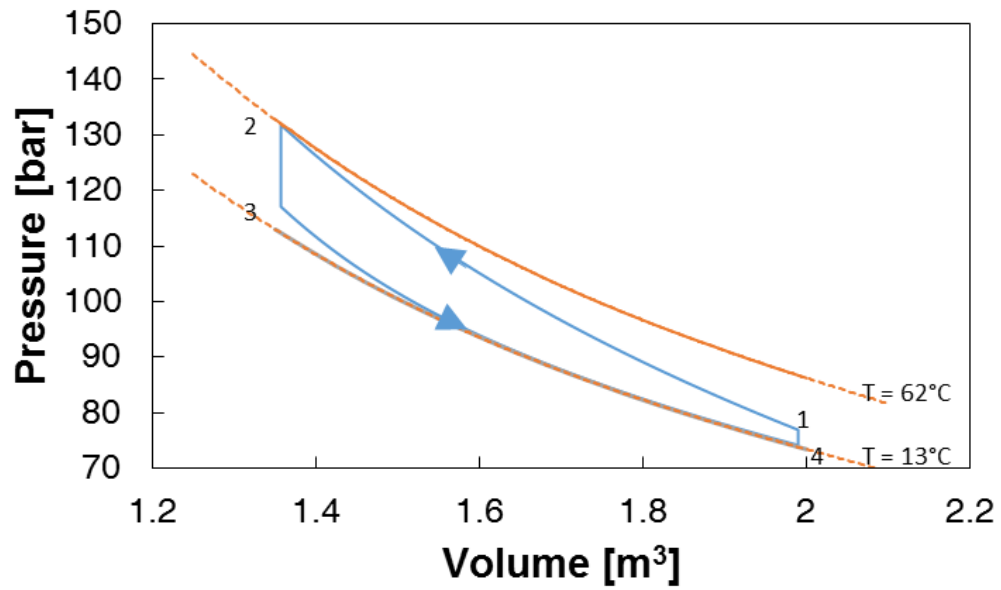
Figure 2, GLIDES 1st generation prototype.

Figure 3, GLIDES base configuration cycle pressure-volume diagram
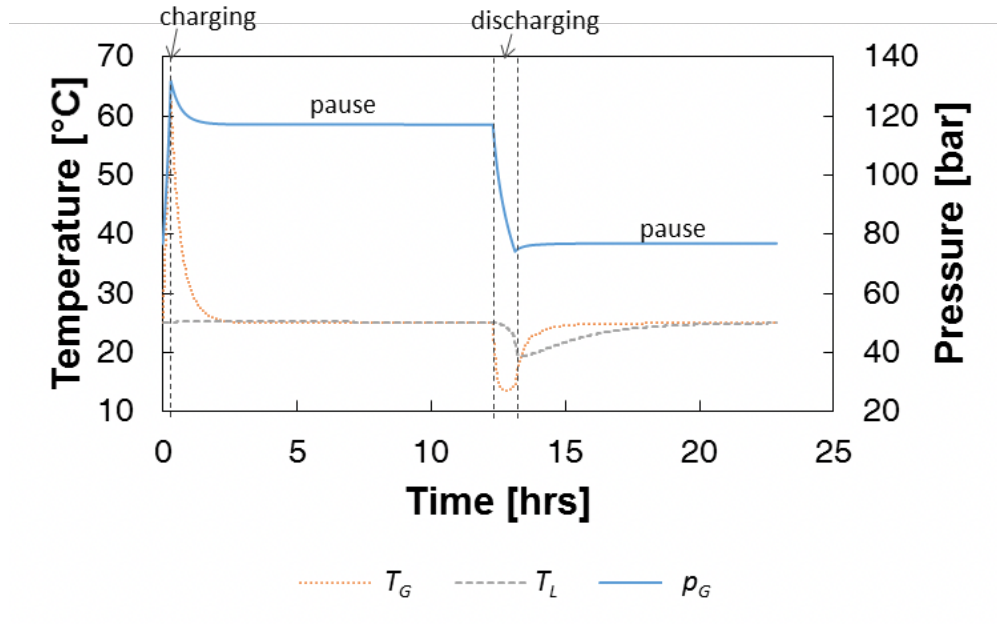
Figure 4, GLIDES base configuration cycle transient temperature and pressure profiles.
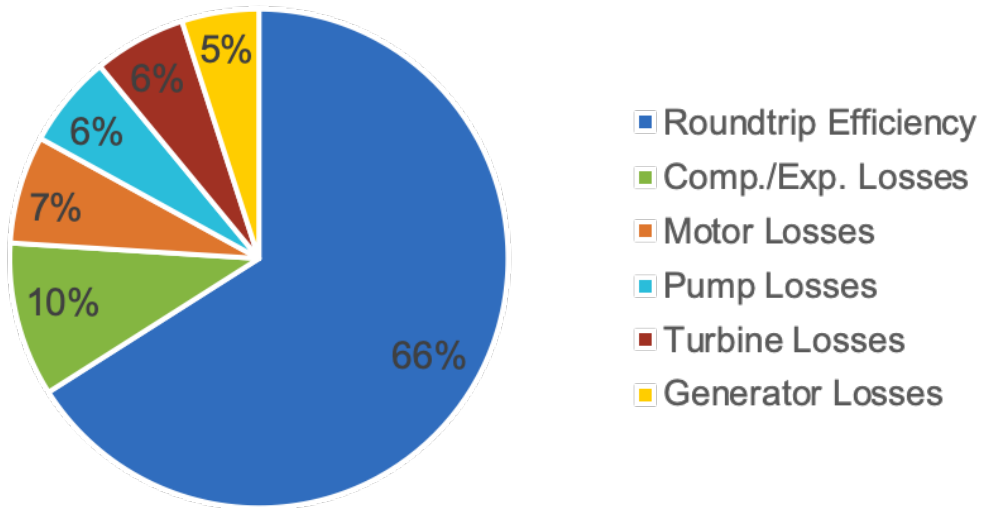

Figure 5, GLIDES base configuration efficiency and losses summary

more complex thermodynamic cycles by controlling the heat transfer rate. To study different scenarios for the GLIDES system and to decrease the losses, multiple GLIDES configurations and heat transfer cycles were studied. As discussed in previous section and as shown in Figure 8, the base configuration of the GLIDES system (the first prototype) is only capable of charging from the bottom of the pressure vessels. Figure 6 shows P-V diagrams for a subset of ideal thermodynamic cycles that can be approached with the GLIDES cycle. In the cycle shown in Figure 6 a), charging occurs isothermally from state 1 to state 2, after which discharging also occurs isothermally back to state 1. In the cycle shown in Figure 6 b), charging is achieved via isothermal compression as the cycle proceeds from state 1 to state 2, then isochoric heat input occurs to state 3, after which the gas expands isentropically back to state 1. In Figure 6 c), process 1-2 is isothermal compression, followed by isobaric heat input to state 3, then isothermal expansion to state 4, and, finally, the system returns to state 1 as isochoric heat removal occurs. The cycle shown in Figure 6 d) is known as a Stirling cycle.

To achieve the heat transfer cycles shown above and to increase the RTE and ED of the system, the second GLIDES prototype with a nominal size of 1 kWh was built at ORNL. As shown in Figure 7, the second GLIDES prototype is a portable and much smaller version of GLIDES which is designed based on the second and third GLIDES studied configurations (Figure 8, explained in the next section). This prototype is capable of charging both from the bottom and top of the pressure vessel and is capable of using excess heat. As shown in Figure 7, the second GLIDES prototype is built using an atmospheric pressure water reservoir, a reversible motor/generator (motor during charging and generator during discharge), a reversible PD hydraulic pump/turbine (pump during charging and turbine during discharge) which can have efficiencies higher than 94%. As explained in previous section, in the first prototype, around 25% RTE is lost due to the
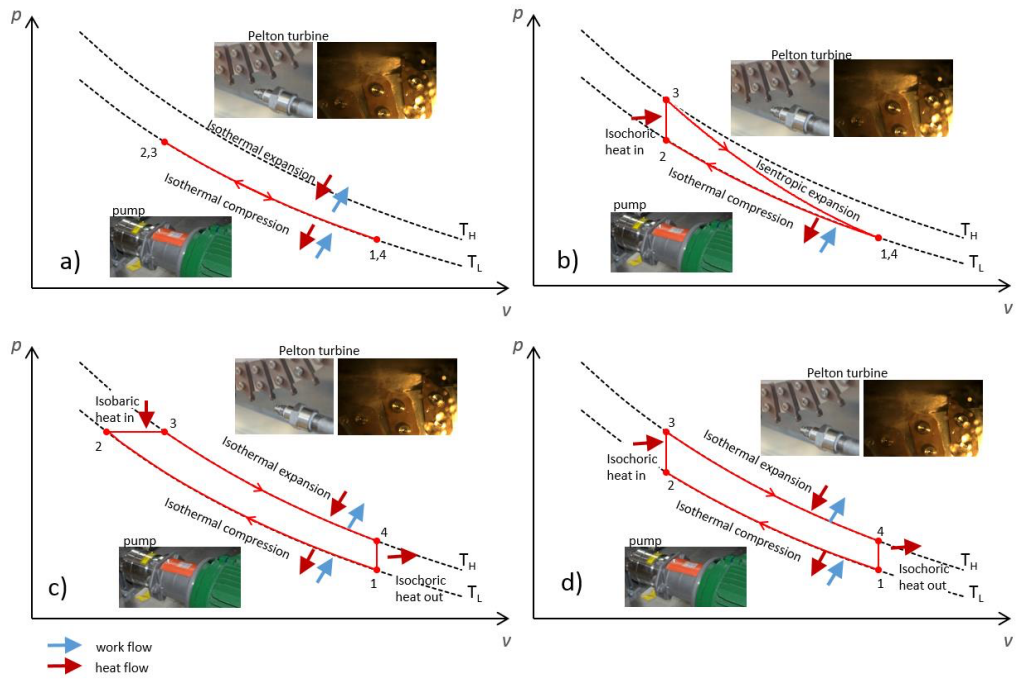
13

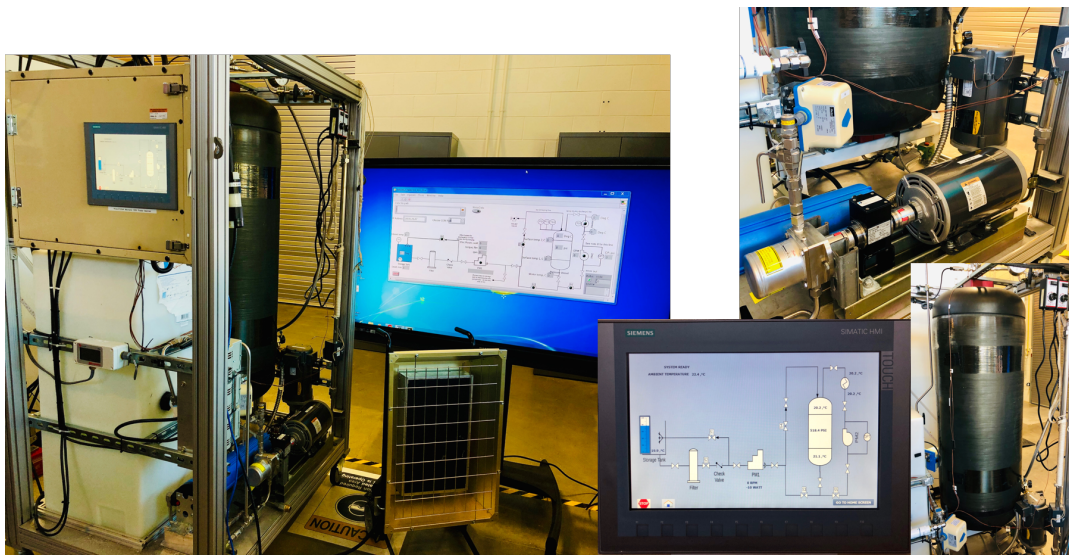Figure 6, Thermodynamic flexibility of the GLIDES concept

Figure 7, GLIDES 2nd generation prototype.

turbomachinery used. To prevent these losses, a perfectly machined turbomachinery (pump/turbine) can be designed, but this would take away the chance to use mass produced machines and therefore increases the cost of the system. Based on the studies done on turbomachinery when building prototypes, it is clear that high turbomachinery efficiencies can be reached and therefore losses can be almost negligible specially when commercialized. Due to this fact, more efforts are put on improving the indicated efficiency and ED of the system.

The best-case scenario for the GLIDES system without using any excess heat, is to have an isothermal compression/expansion cycle as explained in Figure 6 (a). During such cycle, air temperature remains constant allowing more water to be pumped into the pressure vessel before the maximum pressure is reached. One of the configurations studied which is the main subject of this proposal, is to use spray cooling/heating during charging/discharging to achieve isothermal compression/expansion. As explained in previous sections, during charging, the air temperature increases causing losses in the system when water is pumped from the bottom of the pressure vessel (Figure 9 (a)). To decrease this temperature rise, a spray can be used to charge the system from the top of the pressure vessel as shown in Figure 9 (b) (configuration 2, Figure 8).

The previous studies on the first prototype show that because of the large thermal capacity of the water, its temperature experiences a very narrow temperature swing during the entire cycle.

Therefore, the water is cooler than the air during compression and warmer than the air during expansion. Spraying the water into the air provides a favorable cooling effect during charging and warming effect in discharging. As the air temperature drops significantly during the discharge process (Figure 10 (a)), spraying water from the top can decrease this temperature drop in the air. Spraying the water into the air during the discharge can be accomplished by pumping water from

the bottom of the vessel into the top through a spray nozzle and a low-head pump (PM2) as shown in Figure 10 (b).
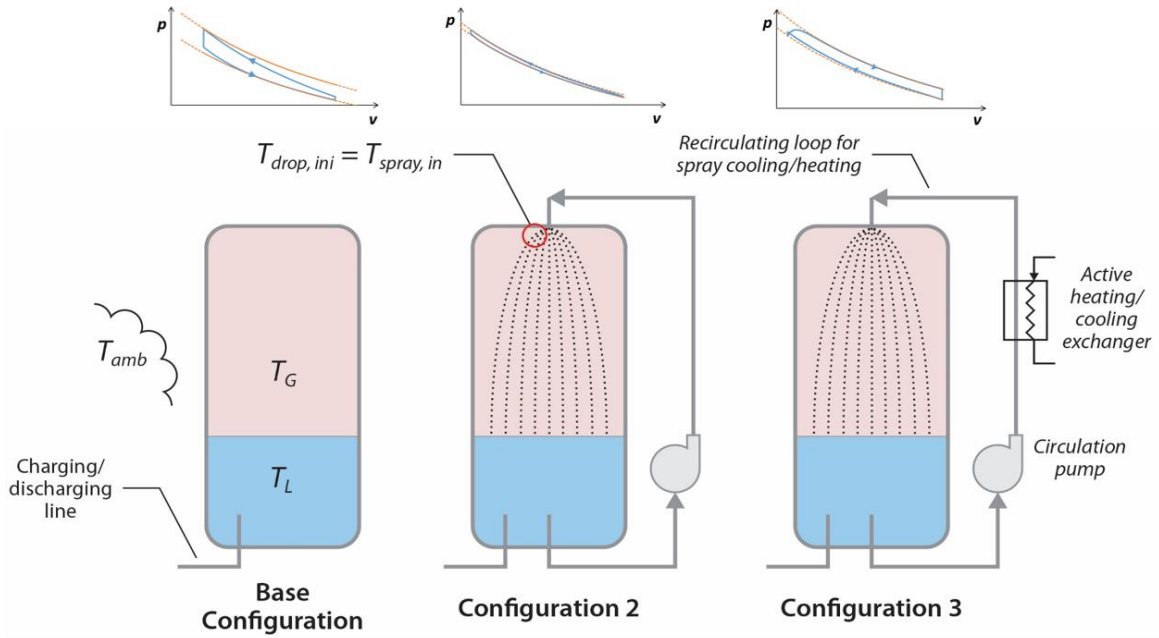
Figure 8, Investigate alternative GLIDES configurations.

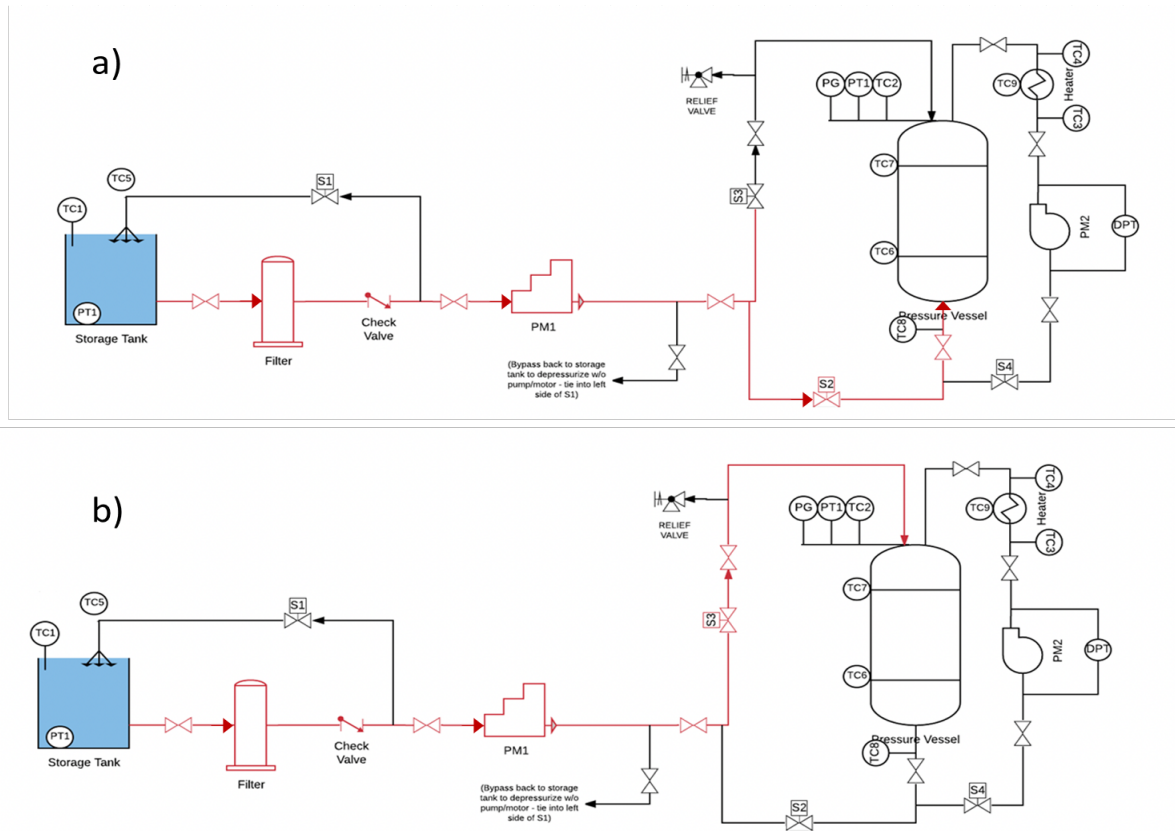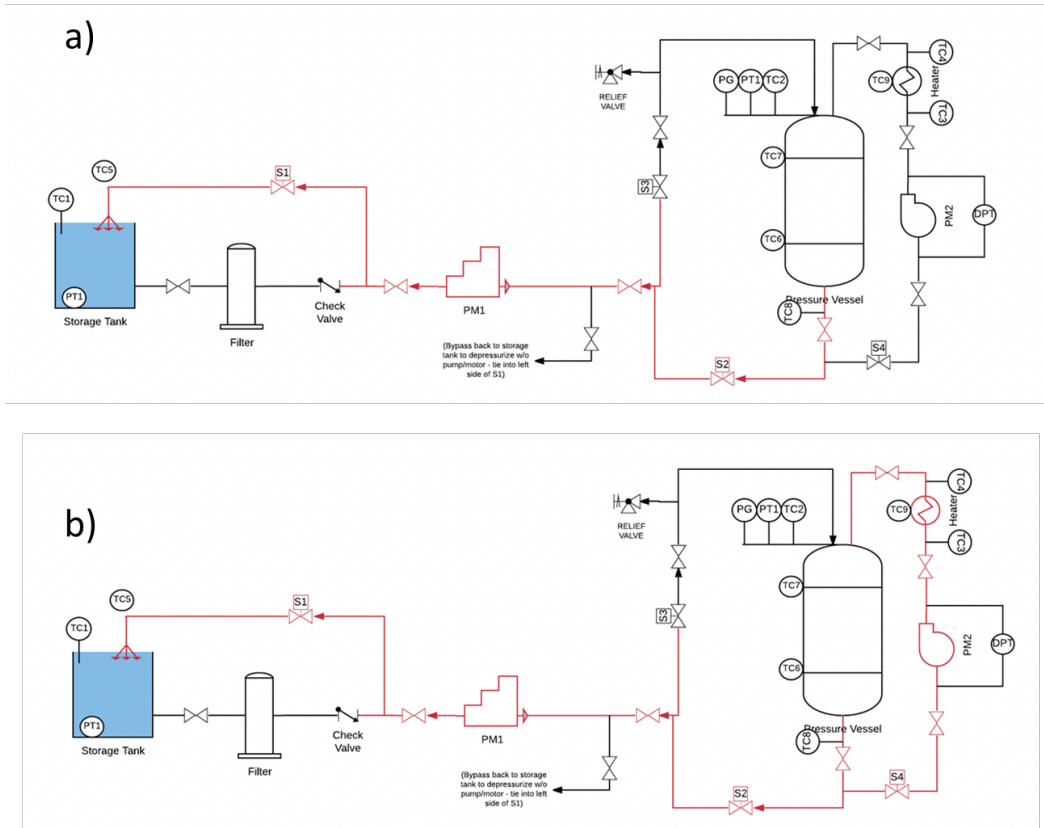Figure 9, GLIDES 2nd generation schematic during charging a) from the bottom, b) from the top.

Figure 10, GLIDES 2nd generation schematic during discharging a) normal discharge, b) with water recirculation and waste heat integration loop active.

Chapter 3: Preliminary Work

3.1 Energy and Heat Transfer Modeling

To analyze the system behavior, an indicated physics-based model is written using MATLAB programming environment. In this section, a detailed overview of this model representing the three major thermal masses (gas, liquid, tank walls) is presented. Figure 11 presents each of the control volumes being considered. The tank walls are modeled as two separate control volumes, the first is the top portion of the tank walls in contact with the gas (T_G). The second is the bottom portion of the tank in contact with the water (T_L). Both control volumes have a dynamic mass that changes as the liquid level changes. Several assumptions are used in the development of this transient model: no spatial temperature gradients within each medium (lumped capacitance), an ambient temperature constant in time, constant thermophysical properties for the tank wall material, modeling of the gas inside the tanks as a Redlich-Kwong (RK) fluid using RK equation of state (for better prediction than an ideal gas at high pressure), negligible heat transfer between the thank upper (T_G) and tank lower (T_L) masses, and all processes occurring at quasi-steady state.

The energy equation for the air is Eq. (1). The term on the left is the time rate of change of the energy contained within the air at time t; the first term on the right is the net rate at which energy is transferred in by heat transfer with the liquid; the second term on the right is the net rate at which energy is transferred in by heat transfer through the tank walls from the ambient; and the last term on the right is the net rate at which energy is transferred out by boundary work.

$$m_G c_{v,G} \frac{dT_G}{dt} = -h_{G,L} A_{G,L}(T_G - T_L) - UA_G(T_G - T_{amb}) - P_G \frac{dV_G}{dt} \qquad (1)$$
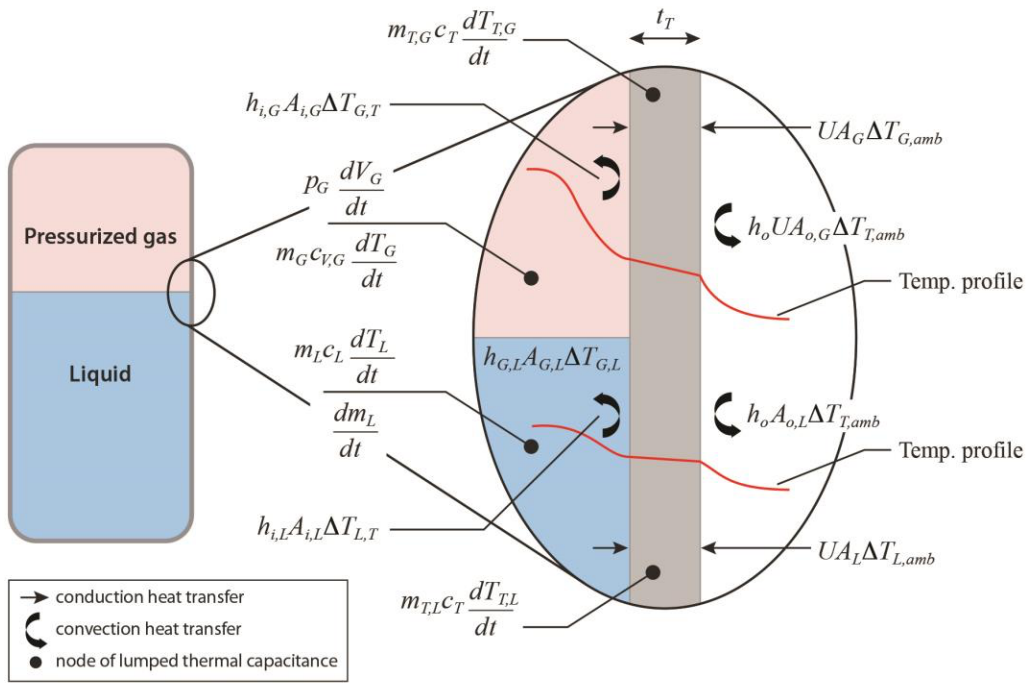
Figure 11, GLIDES physics-based model formulation.

Eqs. (2)-(4) represent the energy equation for the liquid, tank walls in contact with the air, and tank walls in contact with liquid respectively.

$$m_L c_L \frac{dT_L}{dt} = -h_{G,L} A_{G,L}(T_G - T_L) - UA_L(T_L - T_{amb}) + \dot{m}_L c_L(T_{amb} - T_L) \tag{2}$$

$$m_{T,G} c_T \frac{dT_{T,G}}{dt} = h_{i,G} A_{i,G}(T_G - T_{T,G}) - h_0 A_{0,G}(T_{T,G} - T_{amb}) \tag{3}$$

$$m_{T,L} c_T \frac{dT_{T,L}}{dt} = h_{i,L} A_{i,L}(T_L - T_{T,L}) - h_0 A_{0,L}(T_{T,L} - T_{amb}) \tag{4}$$

Eqs. (5) and (6) show the continuity equation for the air and the liquid respectively.

$$\frac{dV_G}{dt} = -\frac{\dot{m}_L}{dt} \tag{5}$$

$$\frac{dm_L}{dt} = \dot{m}_L \tag{6}$$

The overall heat transfer coefficients UA_G and UA_L are calculated using an effective thermal resistance network with convection on the inner surface, conduction through the tank wall, and convection on the outer surface. The resulting expressions are seen in Eqs. (7) and (8).

$$UA_G = \frac{1}{\left(\frac{1}{h_{i,G} A_{i,G}}\right) + \left(\frac{t_T}{K_T A_{ave,G}}\right) + \left(\frac{1}{h_0 A_{0,G}}\right)} \tag{7}$$

$$UA_L = \frac{1}{\left(\frac{1}{h_{i,L} A_{i,L}}\right) + \left(\frac{t_T}{K_T A_{ave,L}}\right) + \left(\frac{1}{h_0 A_{0,L}}\right)} \tag{8}$$

Furthermore, the effect of the direct-contact heat exchange between the air and the liquid obtained via spraying is described. First, it is assumed that a single droplet falls at constant terminal velocity;

therefore, the drag and the gravity forces on each droplet are balanced, and the terminal velocity can be calculated with Eq. (9):

$$v_{term} = \sqrt{\frac{4D_{dr}\rho_{dr}g}{3\rho_G C_D}}$$

(9)

Eq. (10) shows the droplet travel time:

$$t_{trav} = \frac{L(t)}{v_{term}}$$

(10)

Eq. (11) can be used to calculate the number of droplets being generated per unit time.

$$\dot{N}_{dr} = \frac{6\dot{V}_{spr}}{\pi D_{dr}^3}$$

(11)

Using Eq. (12), the total number of droplets of liquid traveling through the air at any given instance in time can be computed.

$$N_{dr} = \dot{N}_{dr} \cdot t_{trav}$$

(12)

Using Eq. (13), the temperature change of a droplet traveling from the top of the vessel to the bulk liquid can be calculated [16]. The temperature of the droplets right before they hit the bulk liquid at the bottom of the tank is calculated (T_{dr}), given the air temperature and the initial temperature of the drop at the outlet of the spray nozzle. Equations (11), (12), and (13) were adapted from Ref. [16], which outlines a procedure for modeling direct-contact heat exchange between air and liquid.

$$\frac{T_{dr,out} - T_G}{T_{dr,in} - T_G} = e^{-\frac{t_{trav}}{\tau_{dr}}}$$

(13)

Eq. (14) shows the thermal time constant of the droplet:

$$\tau_{dr} = \frac{\rho_{dr} V_{dr} c_{dr}}{h_{dr} A_{s,dr}} \tag{14}$$

Next, the Nusselt number for the drops is calculated using the Ranz and Marshall correlation [Eq. (15)] for a falling drop. Development of this Nusselt number correlation is outlined in Ref. [17].

$$Nu_{dr} = 2 + 0.6Re^{1/2} Pr^{1/3} \tag{15}$$

Eq. (16) shows the resulting heat transfer coefficient:

$$h_{dr} = \frac{Nu \cdot k_{dr}}{D_{dr}} \tag{16}$$

Eq. (17) can be used to calculate the heat loss (or gain) from the droplets:

$$Q_{dr} = \rho_{dr} V_{dr} c_{dr} (T_{dr,out} - T_{dr,in}) \tag{17}$$

The rate of heat loss from the entire spray is then calculated as follows in Eq. (18):

$$\dot{Q}_{spr} = \dot{N}_{dr} \cdot Q_{dr} \tag{18}$$

A mixing equation [Eq. (19)] is then applied to calculate the effect of the droplets on the temperature of the bulk liquid at the bottom of the tank. At each time step, the enthalpy of the drops plus the enthalpy of the bulk liquid (pre-mixing) must equal the enthalpy of the combined liquid mixture (droplets plus bulk liquid):

$$T_{L,mixed} = \frac{\dot{m}_{spr}\, \Delta t\, c_{dr} T_{dr} + m_L c_L T_L}{(\dot{m}_{spr}\, \Delta t + m_L) c_L} \tag{19}$$

The effect of this heat transfer is included in the energy balance for the air as shown in Eq. (20):

$$m_G c_{v,G} \frac{dT_G}{dt} = -h_{G,L} A_{G,L}(T_G - T_L) - UA_G(T_G - T_{amb}) - \dot{Q}_{spr} - P_G \frac{dV_G}{dt} \tag{20}$$

3.2 Early-Stage Results

The results from early stage work done on the second GLIDES prototype proves the proposed method can be feasible. Figure 12 shows the P-V diagram of the charging process during compression done by spraying from the top of the vessel. As seen in this plot, the experimental data almost exactly matches the isothermal compression data. As discussed in previous sections, at the end of the compression process, at same air volumes, the air pressure of the experimental data as well as the isothermal process are lower than that of an adiabatic compression. Pressure differences of around 600 psi can be seen in this experiment; meaning (for example) if the maximum working pressure of a carbon fiber pressure vessel was set to around 2,000 psi, if an adiabatic compression was done, only around 180 liters of water could be pumped into the vessel. On the other hand, during an isothermal compression, pumping 180 liters of water into the vessel causes the air pressure to only rise to around 1,200 psi with a margin of around 800 psi to work with. Therefore, this preliminary experiment proves higher amounts of energy can be stored during an isothermal compression than that of an adiabatic compression. Spray heating can be used during the discharge process (expansion) of the GLIDES system using a second pump to circulate the discharging water and spray it from the top to prevent the decrease in air temperature.
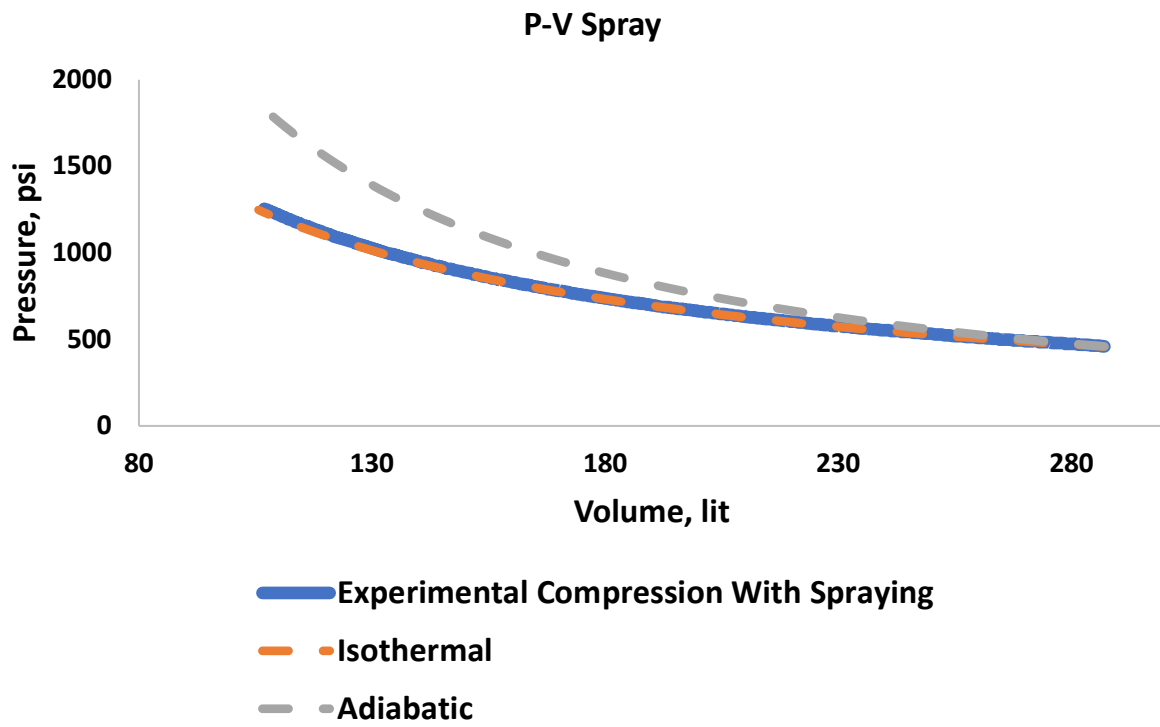
Figure 12, GLIDES compression P-V diagram using spray cooling.

Chapter 4: Milestones/Tasks

- Run full cycles using spray cooling/heating by adding a second pump or likewise options.

- Model an indicated heat transfer model, validate the collected data, and investigate best charging/discharging flow rate using spray charging and spray heating during discharge.

- Integrate excess heat available to boost the RTE.

- Farther research on scalability and ED of GLIDES using condensable gases including CO_2 and other liquids including R134a.

References

[1]   D.   Hollett,   Grid   Modernization   Initiative,   2015. https://www.energy.gov/sites/prod/files/2015/04/f22/DOE Grid Mod Initiative - Lynn.pdf.

[2] U. Energy Information Administration, U.S. Battery Storage Market Trends, Washington, DC, 2018. doi:10.1136/ard.2007.083022.

[3] REN21, Ren21: Renewables 2018 global status report, 2018. doi:978-3-9818911-3-3.

[4] G.J. May, A. Davidson, B. Monahov, Lead batteries for utility energy storage: A review, J. Energy Storage. 15 (2018) 145–157. doi:10.1016/J.EST.2017.11.008.

[5] B. Dunn, H. Kamath, J. Tarascon, Elecfor the Grid : A Battery of Choices, 334 (2011) 928–935. doi:10.1126/science.1212741.

[6] NHA, NHA Pumped Storage Report, Washington, DC, 2018. www.hydro.org.

[7] H. Chen, T.N. Cong, W. Yang, C. Tan, Y. Li, Y. Ding, Progress in electrical energy storage system: A critical review, Prog. Nat. Sci. 19 (2009) 291–312. doi:10.1016/j.pnsc.2008.07.014.

[8] X. Luo, J. Wang, M. Dooner, J. Clarke, Overview of current development in electrical energy storage technologies and the application potential in power system operation, Appl. Energy. 137 (2015) 511–536. doi:10.1016/j.apenergy.2014.09.081.

[9] A.A. Akhil, G. Huff, A.B. Currier, J. Hernandez, D.A. Bender, B.C. Kaun, D.M. Rastler, S.B. Chen, A.L. Cotter, D.T. Bradshaw, W.D. Gauntlett, J. Eyer, T. Olinsky-Paul, M. Ellison, S. Schoenung, DOE/EPRI Electricity Storage Handbook in Collaboration with NRECA, (2016). doi:10.2172/1431469.

[10] U.S. EIA, Annual Energy Outlook 2018 with projections to 2050, Annu. Energy Outlook 2018 with Proj. to 2050. 44 (2018) 1–64. doi:DOE/EIA-0383(2012) U.S.

[11] A. Ulvestad, A Brief Review of Current Lithium Ion Battery Technology and Potential Solid State Battery Technologies, (2018). doi:10.4236/gsc.2012.24020.

[12] O. Krishan, S. Suhag, An updated review of energy storage systems: Classification and applications in distributed generation power systems incorporating renewable energy resources, Int. J. Energy Res. (2018) 1–40. doi:10.1002/er.4285.

[13] M.A. Hannan, M.M. Hoque, A. Mohamed, A. Ayob, Review of energy storage systems for electric vehicle applications: Issues and challenges, Renew. Sustain. Energy Rev. 69 (2017) 771–789. doi:10.1016/j.rser.2016.11.171.

[14] A.O.O. M. Momen, K. J. Gluesenkamp, O. A. Abdelaziz, E. A. Vineyard, A. Abu-Heiba, Near isothermal combined compressed gas/pumped-hydro electricity storage with waste heat recovery capabilities, 15/254,137, n.d.

[15] A. Odukomaiya, A. Abu-Heiba, K.R. Gluesenkamp, O. Abdelaziz, R.K. Jackson, C. Daniel, S. Graham, A.M. Momen, Thermal analysis of near-isothermal compressed gas energy storage system, Appl. Energy. 179 (2016) 948–960. doi:10.1016/j.apenergy.2016.07.059.

[16] F. Cascella and A. Teyssedou, "Modeling a Direct Contact Heat Exchanger used in a supercritical water loop," Applied Thermal Engineering, vol. 79, pp. 132-139, 2015.

[17] W. E. Ranz and W. R. Marshall Jr., "Evaporation From Drops (Part I)," Chemical Engineering Progress, vol. 48, pp. 141-146, 1952.

Vita

Saiid Kassaee was born in Denton, Texas and grew up in Tehran, Iran since he was 2 years old. He moved back to the United States when he was 20 years old with hopes to achieve higher education. During his first two years, he attended Pellissippi State Community College and continued to finish his Bachelor of Science degree in Aerospace Engineering at the University of Tennessee in Knoxville TN. After completing his Bachelor of Science degree, he decided to take a year off from school to give himself some time to decide what his next step would be while working for American Airlines. During his year off, he got the chance to travel round the earth visiting 5 countries. Deciding to pursue higher education, he pursued his PhD in Mechanical Engineering at the University of Tennessee while doing research at Oak Ridge National Laboratory and continued working at American Airlines. His research interests include energy efficiency, energy storage, grid modernization, and compression efficiency. After graduation, he will begin his new position as research and development staff at Oak Ridge National Laboratory. Saiid is incredibly grateful for all the support from his family and friends as he begins his new career.